Available online at

jae.cardiffuniversitypress.org

The Journal of Ammonia Energy 03 (2025) 032–041

Exploring the effect of ammonia enrichment on longitudinal thermoacoustic instability in an annular combustor

Chunyu Liu[a], Haojie Yang[a], Liang Yu[a], Xingcai Lu[a,*]

[a] *Shanghai Jiao Tong University, School of Mechanical Engineering, Shanghai, 200240, PR China*

Abstract

This study investigates the characteristics of thermoacoustic instability in an annular combustor fuelled with ammonia-methane mixtures, with a particular focus on the impact of ammonia enrichment on longitudinal instability. The experiments revealed distinct transitions in combustion states as the equivalence ratio increased from lean to stoichiometric conditions, following the sequence: lean blowout – stable combustion – intermittent oscillation – limit cycle oscillation. Ammonia enrichment was found to reduce oscillation amplitudes while increasing the lean blowout limit. Using integrated experimental diagnostics of acoustic pressure, OH* emissions, flame structure, and phase-averaged flame dynamics, the mechanisms underlying the effect of ammonia addition on thermoacoustic coupling were analysed. The instability maps identified at various equivalence ratios and ammonia content suggested that ammonia addition remarkably weakened the thermoacoustic coupling, which was attributed to the significant increase in convection delay time and ignition delay time by ammonia addition. This work highlights the role of ammonia in mitigating thermoacoustic instability and provides valuable insights for optimizing ammonia-methane combustion systems.

Received: 25th Nov 24; Accepted: 20th Jan 25; Published: 11th April 2025

Keywords: Ammonia combustion, Annular combustion chamber, Thermoacoustic instabilities, Multiple flames, Flame dynamics.

1. Introduction

In recent years, the global pursuit of low-carbon and zero-carbon energy solutions has driven significant advancements in sustainable energy technologies. Among these, ammonia (NH_3) has emerged as a promising zero-carbon fuel, attracting considerable attention from both academia and industry due to its high volumetric energy density, straightforward production processes and well-established transport and distribution infrastructure [1,2]. However, its lower calorific value (316.84 kJ/mol), approximately 39% of that of methane (CH_4, 802.3 kJ/mol) [3], requires higher volumetric flow rates and larger combustion chambers in gas turbines to achieve equivalent energy output. In addition, the low laminar flame speed, challenging ignition characteristics, and relatively low combustion efficiency [4] pose significant challenges to its adoption as a standalone fuel.

To address these limitations, researchers have proposed blending NH_3 with highly reactive fuels, such as H_2 [5,6] or CH_4 [7,8], to improve its combustion properties. Such mixtures increase flame propagation speeds, thereby increasing combustion efficiency and flame stability. Consequently, NH_3-CH_4 mixtures have attracted attention as a fuel that combines energy release, ignition performance, and combustion efficiency [3]. However, in practical gas turbine operation, the application of both pure NH_3 and NH_3-blended fuels faces significant challenges, particularly in achieving stable combustion under complex flow conditions.

Recent studies [4,9] have demonstrated the potential of swirl-stabilized combustion technology to achieve stable NH_3-air flames. By creating a low-velocity recirculation zone within the combustion chamber, this technique effectively improves flame stability. However, the turbulent flows in swirl-stabilized combustors are highly complex, with the presence of vortices, recirculation zones and shear layers often giving rise to various flow instabilities, such as precessing vortex core (PVC) instabilities [10,11] and Kelvin-Helmholtz instabilities [12]. These flow instabilities are closely related to the thermoacoustic instability (TAI) of combustion systems, which is a critical challenge limiting the stable operation of gas turbines [13-15]. TAI arises from the in-phase coupling between the acoustic pressure and the unsteady heat release rate (HRR).

* Corresponding author. Tel.: +86-21-34206039. E-mail address: lyuxc@sjtu.edu.cn
https://doi.org/10.18573/jae.38

Significant progress has been made in understanding the combustion stability of ammonia flames. For example, Elbaz et al. [16] conducted an investigation into the instability and flame structure of NH_3-CH_4-air mixtures stabilized in a combustor featuring a double swirl burner. Their findings demonstrated that cofiring NH_3 and CH_4 in a double concentric swirl burner resulted in a well-defined stable flame regime. Khateeb et al. [17] explored the stability limits of NH_3-CH_4-air swirling flames. They observed that incorporating NH_3 expanded the stable combustion range while minimizing the risk of flashback. Recently, Okafor et al. [18] innovatively developed and tested a highly efficient low-NOx burner designed for liquid ammonia injection. By integrating a multi-nozzle twin-fluid atomizer with a two-stage combustion strategy, this burner achieved highly stable ammonia combustion over a wide range of equivalence ratios, while maintaining low pollutant emissions. Collectively, these studies offer valuable perspectives on the stability behaviour of NH_3 flames. However, experimental investigations and in-depth analyses focusing on the self-excited thermoacoustic instabilities associated with NH_3 combustion remain limited. Currently, Katoch et al. [19] introduced an innovative dual-fuel dual-swirl burner aimed at mitigating thermoacoustic coupling in NH_3-H_2-air flames. Their experimental findings demonstrated that adjusting the degree of mixing between NH_3 and H_2 upstream of the flame zone effectively mitigated thermoacoustic instabilities. In addition, it is well known that the unsteady response of flames to acoustic perturbations is a key mechanism in thermoacoustic instability, which can be evaluated by measuring the flame transfer function (FTF). The FTF consists of two primary components: a gain that decreases with frequency and a phase lag that increases with frequency. Previous studies [20,21] have shown that the laminar flame speed of the fuel has a first-order effect on both components. Furthermore, Wiseman et al. [22] performed the first experimental evaluation of FTFs for turbulently premixed NH_3-H_2-N_2-air flames. Their results demonstrated that, even when the laminar flame speed of the fuel was maintained constant, variations in fuel composition can significantly alter the response of the flame to acoustic perturbations. Recently, Liu et al. [23,24] investigated the TAI characteristics of NH_3-CH_4 flames, revealing potential mechanisms of mode transitions and their sensitivity to swirl intensity variations. In addition, Jin and Kim [25] highlighted the potential of staged combustion strategies to suppress thermoacoustic coupling in NH_3-H_2 flames while reducing NO_x emissions.

Nevertheless, most studies remain focused on single-nozzle combustors. Modern gas turbines typically employ annular combustion systems, where geometric complexity and interactions between multi-nozzle flames significantly complicate the investigation of TAI. In annular combustion systems, the coupling between multiple flames significantly alters the characteristics of combustion instabilities. The response of flames to acoustic excitations differs markedly from that observed in single-nozzle combustors. Therefore, further research is essential to address these challenges and advance the practical application of NH_3-based combustion technologies.

This study addresses these gaps by examining the TAI behaviour of ammonia-enriched flames in annular combustors. The objectives are twofold: (1) to investigate the effect of ammonia enrichment on the longitudinal instability mode of an annular combustor, and (2) to explore the impact of ammonia addition on the neighbouring flame interaction and the unsteady flame dynamics in the presence of TAI. This research provides theoretical insights and practical guidance for optimizing ammonia-based combustion systems in modern gas turbine applications.

2. Experimental setup

Figure 1a shows the schematic of the annular combustor consisting of an air plenum connected to the combustion chamber via twelve equally spaced bluff-body swirl injectors. Premixed fuels and air enter the honeycomb to reduce spatial non-uniformity of gas flow. Each injector has a length of 120 mm with an inner diameter of 20 mm, and is fitted with a centrally located conical bluff-body of 15 mm diameter providing a blockage ratio of 56%. The injector is equipped with an axial swirler. The swirl number based on the swirler dimensions is S_N = 0.78. In the present investigation, the swirlers turn the flow clockwise (CW) when viewed from downstream. Downstream of the combustion chamber, a plug nozzle with a 90% blocked area was installed for creating an acoustically closed boundary and allowing further to adjust the length of the combustion chamber. To excite thermoacoustic instability, the length of the combustion chamber was set at 600 mm throughout the experiments.

The schematic of the diagnostic system is shown in Fig. 1b. Three dynamic pressure sensors (PCB 112A22, 14.61 mV/KPa, uncertainty ± 1%) are positioned 90° apart (marked as M_1, M_2, and M_3 in Fig. 1b) to characterize the instability modes. They were mounted on waveguide tubes positioned 10 cm from the dump plane of the combustion chamber, ensuring a safe distance from the hot wall. Additionally, a Photomultiplier Tube (PMT, CH253) coupled with a bandpass filter (310 ± 10 nm) is employed for capturing OH^* emissions.

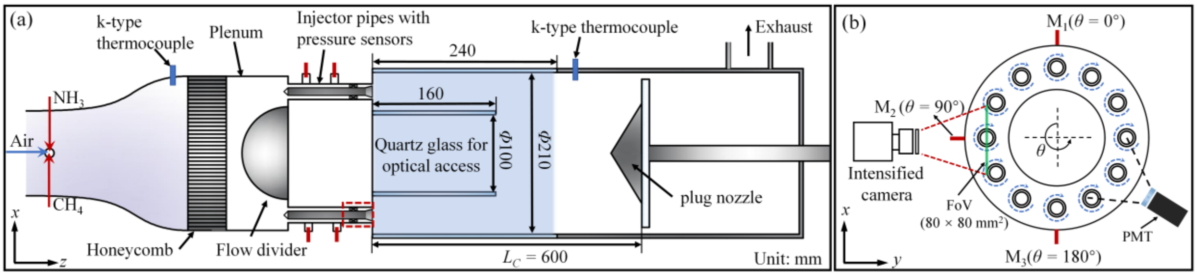

Fig. 1. Schematic drawings of the annular combustor (a) and the diagnostic system (b).

The flame structure is captured by a high-speed CMOS camera (Photron Mini AX 200) with an intensifier (EyeiTS-D-HQB-F). In the study, a total of 4000 images are captured by using a resolution of 1024 × 1024 pixels at 4000 Hz. During the tests, the camera, PMT, and pressure sensors are triggered and synchronized to collect signals.

The experiments were conducted under ambient conditions of 1 atm and 298 K. A summary of the operating conditions is described in Table 1. All tests were performed at a fixed thermal power (P) of 65 kW. The tests cover a broad range of equivalence ratios (ϕ) from 0.7 to 1 with a 0.05 interval. The proportion of ammonia ($X_{\mathrm{NH_3}}$) is defined as the volume fraction in the ammonia-methane mixture, varying from 0 to 0.4. The range of the mixture bulk velocities (U_Z) is 11.6 m/s – 16.3 m/s.

In addition, we conducted a separate set of tests to explore changes in the characteristics of the self-excited combustion instabilities with variations in equivalence ratios. This was investigated by continuous measurements of dynamics pressure (P') and fluctuating heat release rate (HRR). This was performed as follows: the equivalence ratio was gradually decreased from 1.0 until lean blowout (LBO) at a fixed interval ($\Delta\phi$ = 0.02). It should be noted that for each equivalence ratio, 25 s is a refinement step, of which 20 s are used for re-equilibration and 5 s for data acquisition. According to P', the flame undergoes thermoacoustic oscillations when the pressure fluctuations have a distinct characteristic frequency, otherwise the system is taken to be thermoacoustically stable.

Table 1. Operation conditions.

P (kW)	$X_{\mathrm{NH_3}}$	ϕ	U_Z (*m/s*)
65	0, 0.1, 0.2, 0.4	[LBO:0.02:1]	11.6–16.3

3. Results and discussion

3.1 Flame structure

Figure 2 presents direct true-colour images of flames with varying NH_3 concentrations (ϕ = 1), captured using a Nikon D7500 digital camera. The photographs reveal a clear and progressive shift in flame colour, transitioning from blue to orange-yellow as the NH_3 mole fraction increases. This change in coloration is predominantly attributed to the α-band emission of NH_2 radicals, commonly referred to as the "nitrogen glow" phenomenon [26]. The blue hue at lower NH_3 concentrations primarily originates from CH* chemiluminescence, indicative of active hydrocarbon-based reactions, whereas the orange-yellow colour at higher NH_3 levels highlights the increasing dominance of nitrogen-based species in the combustion process.

In addition to the colour transformation, the flame morphology undergoes a noticeable change. As $X_{\mathrm{NH_3}}$ increases, the flame structure anchored on each bluff body in the annular combustion chamber transitions from an M-shaped configuration to a V-shaped one. This morphological shift suggests a weakening of the reaction intensity in the outer recirculation zone (ORZ) of the flame as NH_3 is introduced. The reduced activity in the ORZ can be attributed to the lower reactivity and slower burning velocity of NH_3 compared to hydrocarbon fuels, which diminishes the extent of recirculation-driven mixing and combustion in these zones.

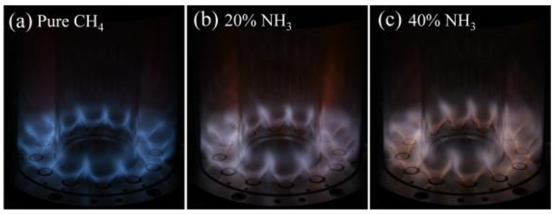

Fig. 2. Time-average broadband photographs of NH_3-CH_4-air flames in the annular combustor under steady operation conditions with ϕ = 1 and P = 65 kW.

3.2. Stability maps

Figure 3 shows the dominant frequency and the corresponding pressure oscillation amplitude measured at M_2 in the (ϕ, $X_{\mathrm{NH_3}}$) domain at P = 65 kW. These iso-contour maps represent constitutive stability features for several relevant parameters. Note that combustion is stable in the white region of the plots. One notes that the frequency of TAI is in the range of 200-230 Hz, correlating with the longitudinal instability mode of the combustor. First, we can observe a significant effect of ammonia addition on the instability characteristics. The frequency decreases with increasing X_{NH_3}. The range of operating conditions for thermoacoustic stability is remarkably widened. Second, the amplitude of pressure oscillations reduces significantly as X_{NH_3} increases. The results suggest that a certain amount of ammonia enrichment can weaken the thermoacoustic coupling in the annular combustion system. However, at X_{NH_3} = 40%, a lower dominant frequency (~80 Hz) is observed, which is different from the acoustic mode of the combustor. This could be an entropy-related instability mode that requires further investigation to determine. This result emphasizes that flames at high X_{NH_3} are prone to exhibit low frequency instability under certain specific conditions, possibly because the slower reaction rate of ammonia enhances the sensitivity of flame to turbulence disturbances.

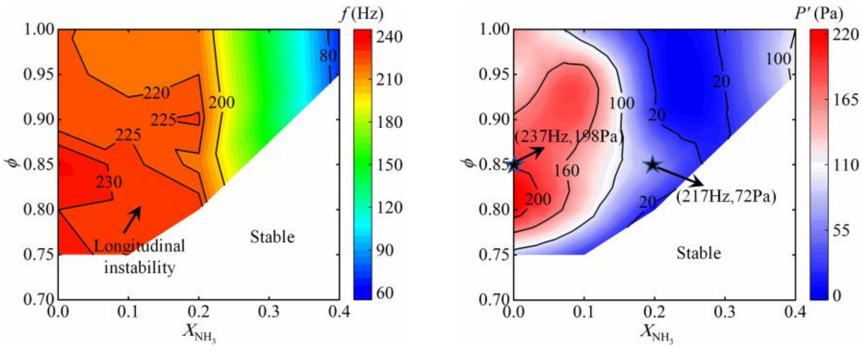

Fig. 3. Illustration of iso-contour instability maps as a function of the X_{NH_3} and ϕ. The instability frequency (left) and pressure oscillation amplitudes (right) are presented at various operation conditions. The white regions mean that the system is thermoacoustically stable.

3.3 Oscillation mode transitions

Figure 4 shows the amplitude of the pressure oscillations at P = 65 kW and the corresponding power spectrogram obtained by continuous wavelet transform (CWT). The results show that the combustion dynamics for both cases show similar trends as the equivalence ratio (ϕ) decreases. Initially, when ϕ is close to 1, the self-excited oscillatory system operates at a relatively low amplitude. However, as ϕ decreases to approximately 0.9, a distinct transition occurs in the combustion system, which abruptly shifts to a higher amplitude unstable state. With further reduction of ϕ, the oscillation amplitude undergoes a further significant decrease and the instability begins to show noticeable intermittency. A similar transition phenomenon was reported in spray flames [27] and stratified flames [28]. Then, the combustion system stabilizes at ϕ close to 0.7. Finally, as ϕ continues to decrease, the flame blows out due to insufficient fuel for sustained combustion. Throughout the process, different types of combustion oscillations can be classified as follows:

(i) Stable combustion: Characterized by the absence of a dominant frequency in the power spectrum.
(ii) Intermittent oscillation: Characterized by low-amplitude pressure oscillations and the intermittent presence of a dominant frequency.
(iii) Limit cycle oscillation: Defined by high amplitude pressure oscillations with the presence of weak secondary harmonic frequencies.

From a dynamical systems perspective, the transition from a stable to an unstable state occurs via a Hopf bifurcation [29]. In certain cases, this bifurcation may follow an intermittent route, influenced by background noise [30,31] or low-dimensional deterministic chaos [32], as observed in our experiments. Notably, the addition of ammonia significantly suppresses the strength of the thermoacoustic oscillations, while leading to a change in the equivalence ratio at which the transition of the oscillation type occurs. These changes are closely related to the combustion chemistry properties of ammonia which will be analyzed in depth in subsequent sections.

Figure 5 illustrates in detail the various combustion states captured in the experiment. The corresponding time series of dynamic pressure and flame intensity fluctuations, spectrum, phase space reconstruction, and recurrence plots are presented to visualize the different combustion states. First, in the stable combustion state, no distinct primary frequency is observed. The trajectories in the reconstructed phase space are chaotic, primarily due to white noise generated by turbulent combustion [33]. Second, for the intermittent oscillation, noticeable intermittent fluctuations in acoustic pressure and flame intensity are observed.

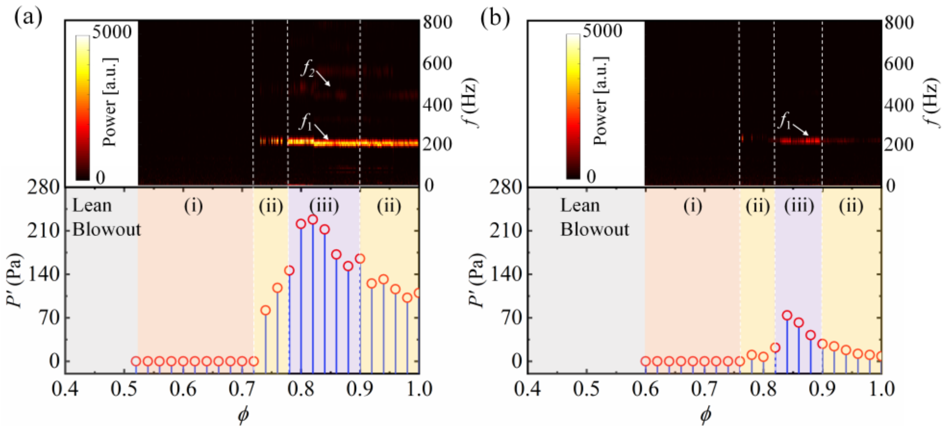

Fig. 4. Overview of the thermoacoustic oscillation characteristics of swirl flames at P = 65 kW, (a) pure CH_4 flame and (b) 20% NH_3 flame.

The recurrence plot exhibits a transition from ordered pressure oscillations to disordered noise patterns. For the limit cycle oscillation, both pressure and flame intensity exhibit stable amplitude periodic oscillations. The oscillation amplitude increases significantly. Furthermore, the reconstructed phase space shows closed-loop trajectories, indicating the system has reached a limit cycle state [34]. Lastly, for the 40% NH_3 mixture at ϕ = 0.95, a multi-frequency mode distinct from the structural acoustic modes is observed. Pressure and flame intensity fluctuations display multiple low-frequency peaks. Due to the diversity of oscillation frequencies, significant distortion in the phase space is evident.

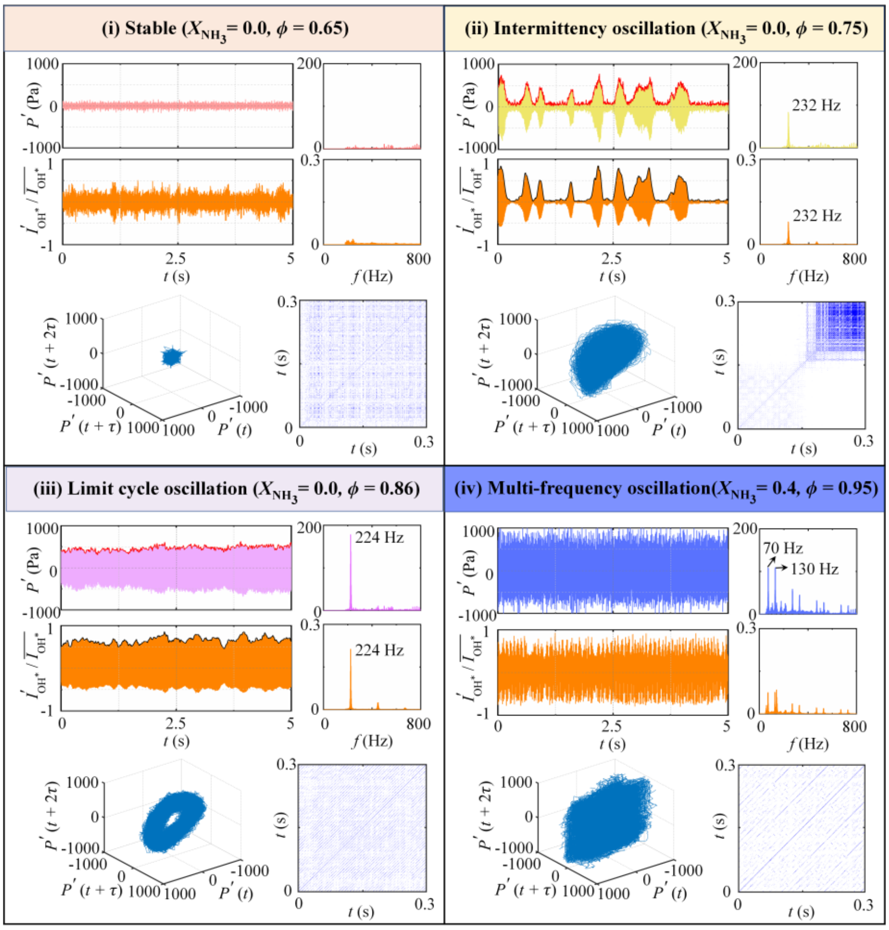

Fig. 5. Pressure and flame intensity fluctuation time series, spectral analysis, phase space trajectories, and recurrence plots for different combustion states.

3.4 Flame dynamics

Next, we selected the two cases marked in Fig. 3 (right) to visualize their flame pulsation characteristics. Figure 6 initially presents their dynamic pressure time series and corresponding spectrum. In both cases, pressure measurements at three locations (M_1 to M_3) exhibit in-phase synchronized oscillations, indicating longitudinal oscillation modes. For pure CH_4 flame, shown in Fig. 6a, high-amplitude pressure and periodic OH* oscillations were detected. The instability frequency was 237 Hz, with a pressure fluctuation amplitude of 198 Pa and a normalized OH* fluctuation amplitude of 0.35. In contrast, the 20% NH_3 flame shows a significantly reduced pressure fluctuation amplitude (72 Pa), with a slightly lower oscillation frequency. Additionally, intermittent flame intensity oscillations are observed in Fig. 6b based on the envelope of the periodic OH* fluctuations.

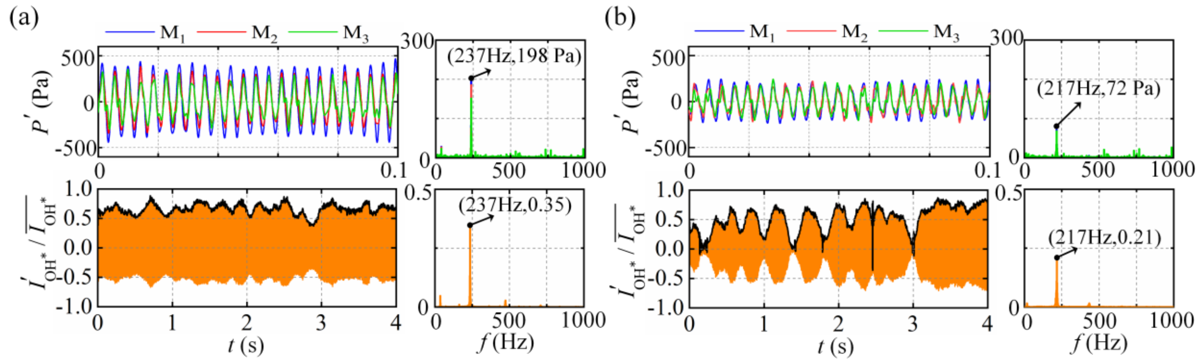

Fig. 6. The time series and spectral analysis of pressure and flame intensity fluctuations for pure CH_4 flame (a) and 20% NH_3 flame (b) at ϕ = 0.85.

Figure 7 illustrates the phase-resolved flame dynamics for the two cases discussed above by phase averaging the captured flame OH* emission images. Time series of pressure fluctuations and normalized OH* fluctuations during an oscillation cycle are also plotted. The black dots in the diagram represent the different phases of the flame within a single oscillation cycle. Firstly, for pure CH_4 and the 20% NH_3 flames, the normalized OH* and pressure oscillation signals exhibit phase differences of approximately 13° and 37°, respectively. This indicates in-phase synchronized oscillations during thermoacoustic instability, consistent with Rayleigh criterion [35]. In the case of pure CH_4, large-amplitude axial flame oscillations are observed. Initially, the flame nearly extinguishes at phase 1. From phase 2 to phase 8, the flame propagates downstream, with OH* intensity peaking at phase 8. The flame subsequently retreats rapidly from phase 9 to phase 12, accompanied by merging and separation in adjacent flame interaction regions. Throughout the oscillation cycle, the flame height undergoes significant variation, representing a pronounced extinguish-reignite oscillation mode. Additionally, distinct flame tail roll-ups are observed at phase 8 and phase 9, suggesting that this oscillation mode is likely governed by vortex dynamics in the flow field.

In contrast, for the 20% NH_3 flame, no significant large-amplitude axial flame motion is observed. Instead, the flame front exhibits minor axial oscillations during the oscillation cycle. This process is accompanied by periodic expansion and contraction of the distance between adjacent flame brushes and forward-backward movement in the flame merging region. One key distinction between the two cases lies in the weaker OH* intensity oscillation in the flame interaction regions for 20% NH_3 flame. Correspondingly, the flame height varies much less significantly, which aligns with the lower pressure oscillation amplitude. Based on the above discussion, it can be inferred that the differences in instability amplitudes between the two cases are primarily attributed to variations in the position and intensity of interactions regions between neighboring flames.

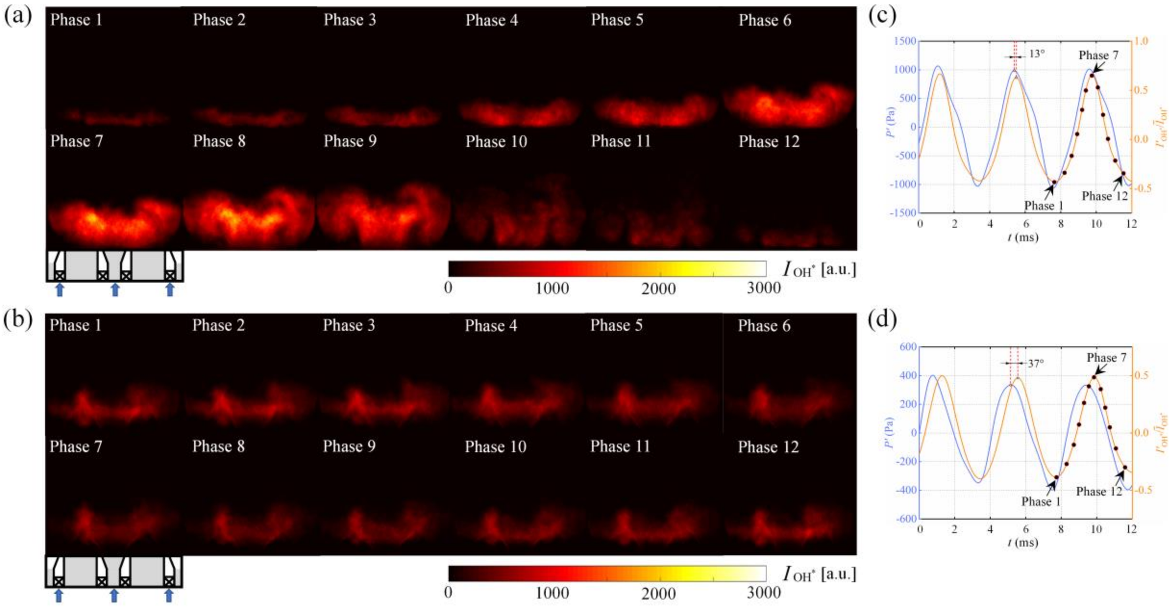

Fig. 7. Phase-averaged flame dynamics for pure CH_4 flame (a) and 20% NH_3 flame at ϕ = 0.85 (b) (left). The time series of pressure and heat release rate fluctuations during an oscillation cycle (right).

The Rayleigh Index (RI) map can provide a quantitative assessment of the coupling between unsteady heat release rate and dynamic pressure fluctuations [36]. The RI is calculated using the following expression:

$$RI(x,y) = T^{-1}\int_0^T P'(x,y)\cdot I'_{OH*}(x,y)\,dt \qquad (1)$$

here T is the oscillation period of the instability, $P'(x,y)$ represents the dynamic pressure fluctuations, and $I'_{OH*}(x,y)$ indicates the heat release rate fluctuations, derived from the intensity of each pixel in OH* images captured by a high-speed camera. A positive RI denotes an acoustically driving region, where pressure and heat release rate oscillations are in-phase, reinforcing each other. Conversely, a negative value indicates an acoustically damping region, where oscillations tend to diminish.

Figure 8 presents the spatially resolved local RI maps for the two cases. First, for pure CH_4 flame, the acoustically driving regions are primarily concentrated in the regions downstream of the flame and the interaction between adjacent flames. These local regions exhibit strong thermoacoustic coupling, contributing significantly to instability. However, for 20% NH_3 flame, the distribution of acoustically driving and damping regions is more dispersed and less intense. The weakening and dispersal of strong coupling zones indicate that the addition of NH_3 reduces the intensity of thermoacoustic coupling. This further confirms the results of the experimental observations.

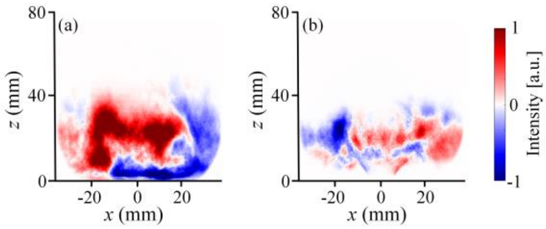

Fig. 8. The spatial distribution of the Rayleigh index for pure CH_4 flame (a) and 20% NH_3 flame (b) at ϕ = 0.85.

3.5 Mechanism analysis

To explore the mechanism of ammonia addition weakening thermoacoustic coupling, two cases described above with frequencies and amplitudes of (237Hz, 198Pa) and (217Hz, 72Pa), respectively, were chosen. It is well known that time delays are very important for the development of TAI. The time delay between the HRR and the pressure determines the amplification or attenuation of instability [35]. The changes in this time delay are linked to changes in convective time delay (τ_{conv}) or chemical reaction time delay (τ_{chem}). The τ_{chem} is related to the ignition delay time (IDT) of fuel, calculated by Chemkin software [37] with the reaction mechanism from the CRECK modeling group [38], as shown in Fig. 9b. It can be found that the increase in ammonia content leads to a significant increase in IDT. For two cases, they are 1.64 ms and 1.76 ms, respectively. Moreover, the adiabatic flame temperature (T_f) was calculated as shown in Fig. 9a. The ammonia enrichment reduces the flame temperature, which can explain the decrease in TAI frequency due to ammonia addition.

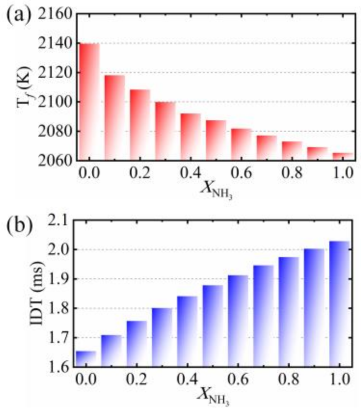

Fig. 9. Calculated adiabatic flame temperatures (a) and ignition delay times (b) for different X_{NH_3}.

For the τ_{conv}, which is the time for the disturbance to travel from the source to the flame centre, it can be estimated based on the flame height (H_f) through the expression [39]:

$$\tau_{conv} = H_f / U_Z \qquad (2)$$

where the H_f was calculated based on the mean flame shape for both cases, as displayed in Fig. 4. The τ_{conv} are 1.45 ms and 1.74 ms for the two cases, respectively. Therefore, it can be inferred that the addition of ammonia increases both the τ_{conv} and the τ_{chem}, leading to an increase in the phase delay between the pressure fluctuations and the heat release rate oscillations, thus weakening the thermoacoustic coupling and ultimately leading to a decrease in the instability amplitude.

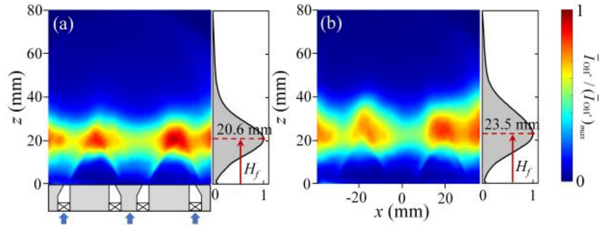

Fig. 10. Mean flame shape at P = 65 kW and ϕ = 0.85 for pure CH_4 flame (a) and 20% NH_3 flame (b).

4. Conclusions

This study experimentally investigated the influence of ammonia addition on thermoacoustic instabilities in a premixed, swirl-stabilized annular combustor. The mechanisms by which ammonia enrichment affected thermoacoustic coupling were explored through flame structure observations, phase-averaged flame evolution, and spatial distribution of the RI. The key findings are summarized as follows:

1. Under fixed combustor length and thermal power conditions, longitudinal thermoacoustic instability modes were observed over a wide range of equivalence ratios. As the equivalence ratio continuously decreased from stoichiometric conditions, various oscillation types were captured. The transition from stable combustion to unstable states occurred through intermittent oscillatory pathways, ultimately progressing to limit cycle oscillations. The bifurcation mechanism remained consistent regardless of ammonia addition, indicating that ammonia enrichment did not significantly alter the transition dynamics.
2. Ammonia enrichment significantly reduced thermoacoustic oscillation amplitudes. For ammonia-enriched flames, weak axial oscillations were observed at the flame tail, contrasting with the fully extinguished-to-reignited oscillatory mode of pure methane flames. These changes primarily manifested as shifts in the position and intensity of interaction regions between neighboring flames. Moreover, the RI distribution revealed stronger thermoacoustic coupling at the flame tail and interaction zones for methane flames, while ammonia-enriched flames exhibited more dispersed and weaker coupling regions.
3. By combining fuel chemical kinetics calculations, it was found that ammonia enrichment increased chemical reaction time delays and convective time delays. These increased delays resulted in greater phase delay between pressure oscillations and heat release rate fluctuations, which in turn weakened thermoacoustic coupling. Consequently, the amplitude of instabilities was significantly reduced, underscoring the dampening effect of ammonia on thermoacoustic instabilities.

In conclusion, this study provides insights into the role of ammonia in weakening thermoacoustic coupling within annular combustion systems. The findings deepen the understanding of the thermoacoustic stabilizing role of ammonia, offering valuable guidance for the development of stable, ammonia-enriched gas turbine combustion technologies.

Acknowledgments

The authors gratefully acknowledge the financial support from the National Natural Science Foundation of China (No. W2411043).

Conflicts of Interest

The authors declare no conflict of interest.

References

[1] Valera-Medina A., Xiao H., Owen-Jones M., David W.I.F., Bowen P.J. Ammonia for power.

Prog Energy Combust Sci 2018; 69: 63–102. https://doi.org/10.1016/j.pecs.2018.07.001
[2] Kobayashi H., Hayakawa A., Somarathne K.D.K.A., Okafor E.C. Science and technology of ammonia combustion. Proc Combust Inst 2019; 37: 109–133. https://doi.org/10.1016/j.proci.2018.09.029
[3] Ariemma G.B., Sorrentino G., Ragucci R., Joannon M., Sabia P. Ammonia/Methane combustion: Stability and NOx emissions. Combust. Flame 2022; 241:112071. https://doi.org/10.1016/j.combustflame.2022.112071
[4] Okafor E.C., Somarathne K.D.K.A., Hayakawa A., Kudo T., Kurata O., Iki N., Kobayashi H. Towards the development of an efficient low-NOx ammonia combustor for a micro gas turbine. Proc Combust Inst 2018; 37: 4597–4606. https://doi.org/10.1016/j.proci.2018.07.083
[5] Li B., Fernández-Galisteo D., Sánchez A.L., Williams F.A. Systematically derived reduced kinetics for hydrogen/ammonia gas-turbine combustion. Combust Flame 2024; 269: 113698. https://doi.org/10.1016/j.combustflame.2024.113698
[6] Zhang F, Zhang G, Wang Z, Wu D, Jangi M, Xu H. Experimental investigation on combustion and emission characteristics of non-premixed ammonia/hydrogen flame. Int J Hydro Energy 2024; 61: 25–38. https://doi.org/10.1016/j.ijhydene.2024.02.281
[7] Kurata O., Iki N., Matsunuma T., Inoue T., Tsujimura T., Furutani H., Kobayashi H., Hayakawa A. Performances and emission characteristics of NH_3-air and NH_3CH_4-air combustion gas-turbine power generations. Proc Combust Inst 2016; 36: 3351–3359. https://doi.org/10.1016/j.proci.2016.07.088
[8] Xiao H., Valera-Medina A., Bowen P.J. Study on premixed combustion characteristics of co-firing ammonia/ methane fuels. Energy 2017; 140: 125–135. https://doi.org/10.1016/j.energy.2017.08.077
[9] Okafor E.C., Yamashita H., Hayakawa A., Somarathne K.D.K.A., Kudo T., Tsujimura T., Uchida M., Ito S., Kobayashi H. Flame stability and emissions characteristics of liquid ammonia spray co-fired with methane in a single stage swirl combustor. Fuel 2021; 287: 119433. https://doi.org/10.1016/j.fuel.2020.119433
[10] Syred N. A review of oscillation mechanisms and the role of the precessing vortex core (PVC) in swirl combustion systems. Prog Energy Combust Sci 2006; 32: 93–161. https://doi.org/10.1016/j.pecs.2005.10.002
[11] Karlis E., Liu Y., Hardalupas Y., Taylor A.M.K.P. Extinction strain rate suppression of the precessing vortex core in a swirl stabilised combustor and consequences for thermoacoustic oscillations. Combust. Flame 2020; 211: 229–252. https://doi.org/10.1016/j.combustflame.2019.09.031
[12] Deng X.-D., Jia B.-Q., Cui X., Wang N.-F., Shi B.-L. Temporal Instability of Liquid Jet in Swirling Gas with Axial Velocity Oscillation. AIAA J 2022; 60: 3852–3862. https://doi.org/10.2514/1.J061082
[13] Huang Y., Yang V.. Dynamics and stability of lean-premixed swirl-stabilized combustion. Prog Energy Combust Sci 2009; 35: 293–364. https://doi.org/10.1016/j.pecs.2009.01.002
[14] Poinsot T. Prediction and control of combustion instabilities in real engines. Proc Combust Inst 2016; 36: 1–28. https://doi.org/10.1016/j.proci.2016.05.007
[15] Zhao D. Transient growth of flow disturbances in triggering a Rijke tube combustion instability. Combust. Flame 2012; 159: 2126–2137. https://doi.org/10.1016/j.combustflame.2012.02.002
[16] Elbaz A.M., Albalawi A.M., Wang S., Roberts W.L. Stability and characteristics of NH_3/CH_4/air flames in a combustor fired by a double swirl stabilized burner. Proc Combust Inst 2023; 39: 4205–4213. https://doi.org/10.1016/j.proci.2022.06.004
[17] Khateeb A.A., Guiberti T.F., Zhu X., Younes M., Jamal A., Roberts W.L. Stability limits and exhaust NO performances of ammonia-methane-air swirl flames. Exp Therm Fluid Sci 2020; 114: 110058. https://doi.org/10.1016/j.expthermflusci.2020.110058
[18] Okafor E.C., Kurata O., Yamashita H., Iki N., Inoue T., Jo H., Shimura M., Tsujimura T., Hayakawa A., Kobayashi H. Achieving high flame stability with low NO And Zero N_2O and NH_3 emissions during liquid ammonia spray combustion with gas turbine combustors. Proc Combust Inst 2024; 40: 105340. https://doi.org/10.1016/j.proci.2024.105340
[19] Katoch A., Guiberti T.F., de Campos D.V., Lacoste D.A. Dual-fuel, dual-swirl burner for the mitigation of thermoacoustic instabilities in turbulent ammonia-hydrogen flames. Combust. Flame 2022; 246:112392. https://doi.org/10.1016/j.combustflame.2022.112392
[20] Æsøy E., Aguilar J.G., Bothien M.R., Worth N.A., Dawson J.R. Acoustic-Convective Interference in Transfer Functions of Methane/Hydrogen and Pure Hydrogen Flames. J Eng Gas Turbines Power 2021; 143(12): 121017. https://doi.org/10.1115/1.4051960
[21] Duarte Nunes C., Morgans A. The Acoustic Response of Hydrogen/Ammonia Flames. Journal

of Ammonia Energy 2023; 1(1). https://doi.org/10.18573/jae.15
[22] Wiseman S., Gruber A., Dawson J.R. Flame Transfer Functions for Turbulent, Premixed, Ammonia-Hydrogen-Nitrogen-Air Flames. J. Eng. Gas Turbines Power 2022; 145: 031015. https://doi.org/10.1115/1.4055754
[23] Liu C., Yang H., Ruan C., Yu L., Nan J., Li J., Lu X. Experimental study on effects of ammonia enrichment on the thermoacoustic instability of lean premixed swirling methane flames. Fuel 2024; 357: 129796. https://doi.org/10.1016/j.fuel.2023.129796
[24] Liu C., Yang H., Ruan C., Yu L., Lu X. Influence of swirl intensity on combustion dynamics and exhaust emissions in an ammonia-enriched premixed swirl-stabilized methane/air combustor. Phys. Fluids 2024; 36: 034123. https://doi.org/10.1063/5.0196764
[25] Jin U., Kim K.T. Hybrid rich- and lean-premixed ammonia-hydrogen combustion for mitigation of NOx emissions and thermoacoustic instabilities. Combust. Flame 2024; 262: 113366. https://doi.org/10.1016/j.combustflame.2024.113366
[26] Strutt R.J. The Ammonia Flame. Nature 1912; 89: 320–320. https://doi.org/10.1038/089270a0
[27] Vignat G., Durox D., Prieur K., Candel S. An experimental study into the effect of injector pressure loss on self-sustained combustion instabilities in a swirled spray burner. Proc. Combust. Inst. 2019; 37: 5205–5213. https://doi.org/10.1016/j.proci.2018.06.125
[28] Wang X., Han X., Song H., Yang D., Sung C.-J. Multi-bifurcation behaviors of stability regimes in a centrally staged swirl burner, Phys. Fluids 2021; 33: 095121. https://doi.org/10.1063/5.0063562
[29] Sujith R.I., Pawar S.A. Thermoacoustic Instability: A Complex Systems Perspective. Springer, Switzerland, 2021.
[30] Lieuwen T.C. Experimental investigation of limit-cycle oscillations in an unstable gas turbine combustor. J. Propuls. Power 2002; 18 (1): 61–67. https://doi.org/10.2514/2.5898
[31] Bonciolini G., Faure-Beaulieu A., Bourquard C., Noiray N. Low order modelling of thermoacoustic instabilities and intermittency: flame response delay and nonlinearity. Combust. Flame 2021; 226: 396–411. https://doi.org/10.1016/j.combustflame.2020.12.034
[32] Seshadri A., Nair V., Sujith R.I. A reduced-order deterministic model describing an intermittency route to combustion instability. Combust. Theory Model. 2016; 20 (3): 441–456. https://doi.org/10.1080/13647830.2016.1143123
[33] Wang X., Han X., Wang J., Du J., Sung C.-J. Flame stabilization and thermoacoustic instability during operating condition modulations: Roles of pilot and main flames. Phys. Fluids 2022; 34: 125102. https://doi.org/10.1063/5.0128756
[34] Ma J., Hui X., Han M., Han X., Wang X., Wang J., Chi Z. Influence of the co- and counter-swirl on combustion instability of the centrally staged combustor. Phys. Fluids 2023; 35: 087127. https://doi.org/10.1063/5.0157777
[35] Rayleigh L. The Explanation of Certain Acoustical Phenomena. Nature 1878; 18: 319−321. https://doi.org/10.1038/018319a0
[36] Sun Y., Zhao D., Ji C., Zhu T., Rao Z., Wang B. Large-eddy simulations of self-excited thermoacoustic instability in a premixed swirling combustor with an outlet nozzle. Phys. Fluids 2022; (4): 044112. https://doi.org/10.1063/5.0087055
[37] CHEMKIN-PRO 15131, Reaction Design, San Diego, 2013.
[38] T.C.M. Group, Chemical reaction mechanism for C1-C3 + NO_X (Version 2003, March 2020). https://creckmodeling.chem.polimi.it/menu-kinetics/menu-kinetics-detailed-mechanisms/107-category-kinetic-mechanisms/400-mechanisms-1911-c1-c3-ht-nox.
[39] Bernier D., Lacas F., Candel S. Instability mechanisms in a premixed prevaporized combustor. J. Propuls. Power 2004; 20: 648–656. https://doi.org/10.2514/1.11461